

Economic Priority Map for Horizontal Geothermal Heat Pump Installation Using R600a as a Natural Refrigerant

Montazeri, Mojtaba; Mohammadiun, Mohammad⁺; Mohammadiun, Hamid*⁺;*

Dibae Bonab, Mohammad Hossein; Sadi, Meisam

*Department of Mechanical Engineering, Shahrood Branch, Islamic Azad University,
Shahrood, I.R. IRAN*

ABSTRACT: Growing attention to the Geothermal Heat Pump (GHP) system highlights the necessity of using the technology in an optimized way. Since geographic and meteorological conditions have substantial effects on the efficiency of GHP, a technical and economic feasibility study on a regional scale was performed on residential buildings using R600a as a natural refrigerant. The investigation consists of numerical modeling and enhancement of Horizontal Geothermal Heat Pump Systems (HGHP) by a meta-heuristic algorithm, spatial cooling/heating design load calculation, and regional data exploration to attain a priority map based on economic factors of 96 geographical points in Iran as a case study. The modeling and optimization approach validation was investigated by comparing the computed results with those published in references. Particle Swarm Optimization (PSO) was used as an optimization tool due to its simplicity and accuracy. The effects of geographical factors, including heating & cooling load, cooling to heating load ratio, and different soil types on the objective function, and Total Yearly Cost (TYC) were presented in a table and investigated to have a better picture in a general exploration study. Finally, Iran's HGHP priority map was accurately presented in this study to help policymakers with decisions concerning technology subsidization. This map helps the investigators to have a better picture of the total affecting parameters on GHP system installation.

KEYWORDS: Horizontal geothermal heat pump, Meta-heuristic Optimization; Economic and thermodynamic modeling, R600a refrigerant; Shallow geothermal energy.

INTRODUCTION

The Paris Agreement's climate objective of limiting the rise in the global average temperature well below 2°C above pre-industrial levels while managing to restrict the temperature increase to 1.5 °C requires net-zero and possibly harmful global greenhouse gas emissions by 2055-2080 [1]. Global buildings have led to 30-40%

of final energy use and have resulted in 40 percent of overall carbon dioxide being released directly and indirectly [2]. By 2050, according to the current energy usage and emission intensity, the carbon emission caused by the building sector for heating and cooling purposes will increase up to 50% [3]. Geothermal Heat Pump System

* To whom correspondence should be addressed.

+ E-mail: mmohammadiun@iau-shahrood.ac.ir & hmohammadiun@iau-shahrood.ac.ir
1021-9986/2022/10/3408-3425 18/\$/6.08

(GSHP), among other heating and cooling applicants, takes advantage of the stable ground temperature to save energy and decrease CO₂ emission. GSHP systems attract more attention because they can achieve a higher system performance than the conventional air-source heat pump system [4]. During the last years, the interest in GSHP for satisfying the increasing demand of energy consumption for heating, ventilation, and air conditioning applications has drastically grown in some countries due to its promising advantages over other HVAC systems. Nevertheless, the development of GSHP is still in its early stages [5]. The significant benefits of GSHP could be considered as [6, 7]:

- Low energy consumption with high efficiency
- Not facing energy source intermittency problems
- No need for Intelligent systems with simple design
- Meeting almost all sustainability preconditions

One of the significant barriers in the GSHP systems' extensive development is the system implementation's high initial cost, limiting their market growth [8]. The initial cost payback period may be so long or uncertain depending on the affecting parameters and building thermal requirement [6] even twenty-two years in exceptional cases like in hot, dry climates [9]. One of the significant actions that may boost the development of this sustainable application is to bankroll the GSHP implementation, similar to subsidization programs with which many other states' governments or countries have provided [10, 11]. The operating expenses of a ground source heat pump are fundamentally influenced by the cost of power, fuel prices, the efficiency of the system, the climatic conditions, and finally, the system running time/condition [12, 13]. Accordingly, regional-scale economic-based modeling and exploration have seemed to be mandatory for priority-level appraisal of each city that should be financed. *Somogyi et al.* [14] investigated Shallow Geothermal Energy (SGE) and its sustainable employment in the European Union's selected countries and compared the results to geothermal heat pumps' regulation. They have concluded that mapping shallow geothermal potential based on a Geographic Information System (GIS) could be an appropriate tool for deciding on investments, including vertical GHSP systems with both closed and open-loop specifications. Besides, *Ondreka et al.* [15] have proposed a set of potential maps that help decision-makers with planning and marketing tools regarding

borehole heat exchangers. They have suggested that this mapping type is a helpful tool for picking appropriate geographical points for SGE applications. *Galgaro et al.* [16] have proposed a technique to include regional-scale geotemperature potential maps for SGE systems. The eventual outcome was the outline of the most intense ground heat exchangeable across the unit region, measured based on local topographical and environmental factors, commonplace reference private building energy needs, and efficiency of heat pump energy needs. Apart from the outline of geotemperature potential, few more thematic maps have been produced and analyzed.

A few of them (maps of shallow geothermal heat flow and thermal conductivity) have been acquired by data interpolation in the GIS system by extending the accessible, considerate data to the entire region. *Nam and Ooka* [17] have proposed an experimental approach to generate maps of the geothermal energy exchange potential for shallow vertical closed-loop frameworks.

This technique utilizes both geological and technological data. The ground parameters that mainly affect the heat exchange in borehole heat exchangers, the energy parameters contributing to geothermal systems' activity, and the prerequisites for the heating and cooling of ordinary private buildings have been considered. Spatial modeling was used in the Geographic Information System, leading to a viable and user-friendly computerized cartographic apparatus.

In addition, it was shown that the technique was applied to four regions of southern Italy. *Blum et al.* [18] examined how the design and functionality of vertical GSHP systems are influenced by technological and economic factors and evaluated the spatial relationship these elements have with geographical aspects such as geology and climate conditions. The results suggest that in the layout and implementation of small-scale GSHP systems, the subsurface characteristics are not satisfactorily assessed, leading to under- or over-sizing and, therefore, a long-term effect on the support costs and payback period of the systems.

In this investigation, the regional, average, and a general amount of Carbon Dioxide savings of about 1000 implemented HGHP systems were estimated. As a reaction to the shortage of SGE administration systems, *Alcaraz et al.* [19] have proposed a methodology that sets up a common framework for administering this resource *via* the utilization of the SGE use rights market.

The most critical component of this platform is the geospatial database that appreciates some merits, which are as follows: the proficient administration of a vast number of diverse sorts of geological, hydrogeological, and geothermal data, the plausibility of questioning and visualizing data at the same time, encouraging advanced geothermal investigation, a succinct view of the subsurface system's thermal regime, and in the end an efficient preprocessing of data together with many GIS devices.

Gemelli et al. [20] demonstrated using a Low-Temperature Geothermal Energy (LTGE) energetic economic model based on GIS in the Italian Marche region. The model demonstrates an inactive decision support system for arranging the use of LTGE. The study is inventive in integrating physical and economic variables on a strategic scale for economic analysis for this instrument. The model contains thematic maps of the major indexes of the economy.

The model has also been developed to help house heating decision-making for households, open organizations, and venture capitalists working in geothermal energy. The evaluation of its adaptation to existing economic trends and regulatory guidelines has been taken into account for developing this model.

Sivasakthivel et al. [21] used Taguchi and efficiency approaches to optimize eight critical measures of GHX (ground heat exchanger) used for space heating needs (i.e., rate of mass flow, borehole span, grout conductivity, entering water temperature, warming stack, removal between U tubes, U tube thermal conductivity, and the span of U tube). The target functions are the length of GHX, COP (performance coefficient), and thermal tolerance of GHX.

From Taguchi optimization analysis, the optimum GHX length, COP, and thermal tolerance were calculated. *Robert and Gosselin* [22] have presented a numerical model and optimizing technique to design and estimate the size of vertical GSHP systems minimizing the overall costs, including initial investment and operations costs. They believed the most fundamental factors influencing the overall costs are the number of boreholes and depth. The geothermal heat pumps' energy supply was also assessed by *Blázquez et al.* [23] considering Electric heat pumps and gas engine heat pumps. They have concluded that the only

scenario regarding the nearly zero-energy buildings' (nZEB) requirements in one area are an Electric heat pump system is the water-mixed only system that respects. Additionally, the techno-economic models for the horizontal ground heat exchangers were reviewed by *Cui et al.* [24]. In this study, the analytical and numerical models were generalized by various approaches, and the economic models were designed based on various economic indices. Finally, *Sanaye and Niroomandc* [25, 26] have presented optimized optimizing GSHP systems techniques with both horizontal and vertical ground exchangers, which is the base element of this study. The best choice design factors of GSHP have been calculated by finding the minimum of a predefined function, the entire investment, and process costs, limited to a set of constraints, which is applied to the PSO optimization method. An Empirical investigation of a modified gas engine heat pump in heating and cooling mode for the residential application has been investigated by *Varamarzyar et al.* [42] laminar forced convection heat transfer in the rectangular and circular mini channel heat sinks and the heat transfer and pressure drop characteristics for various Reynolds number have been analyzed by *Ghasemi et al.* [43] energy, exergy, and expert economic analysis on the recent trend of joint production of liquefied natural gas and natural gas liquids based on Mixed fluid cascade most important refrigeration systems has been performed by *Khajehpour et al.* [44] a comparative study and multi-objective optimization of various configurations in the natural gas liquefaction process has been presented by *Ahmadi et al.* [45].

To generate a priority map based on economic factors for a group of defined cities in Iran with different climate conditions, a thermodynamic model and the optimizing PSO method were developed in this study. For the heating cycle, the graphical view of the HGHP system may be seen in Fig. 1. A closed-loop framework containing water-mixed antifreeze radiator fluid absorbs heat from the ground. Following that, energy-carrying fluid exchanges the energy to the refrigerant within the heat pump's evaporator heat exchanger. The refrigerant is vaporized and then compressed within the compressor. Hot refrigerant enters a heat exchanger called a condenser and transfers its energy to the medium. For cooling mode, the system goes through a reverse cycle.

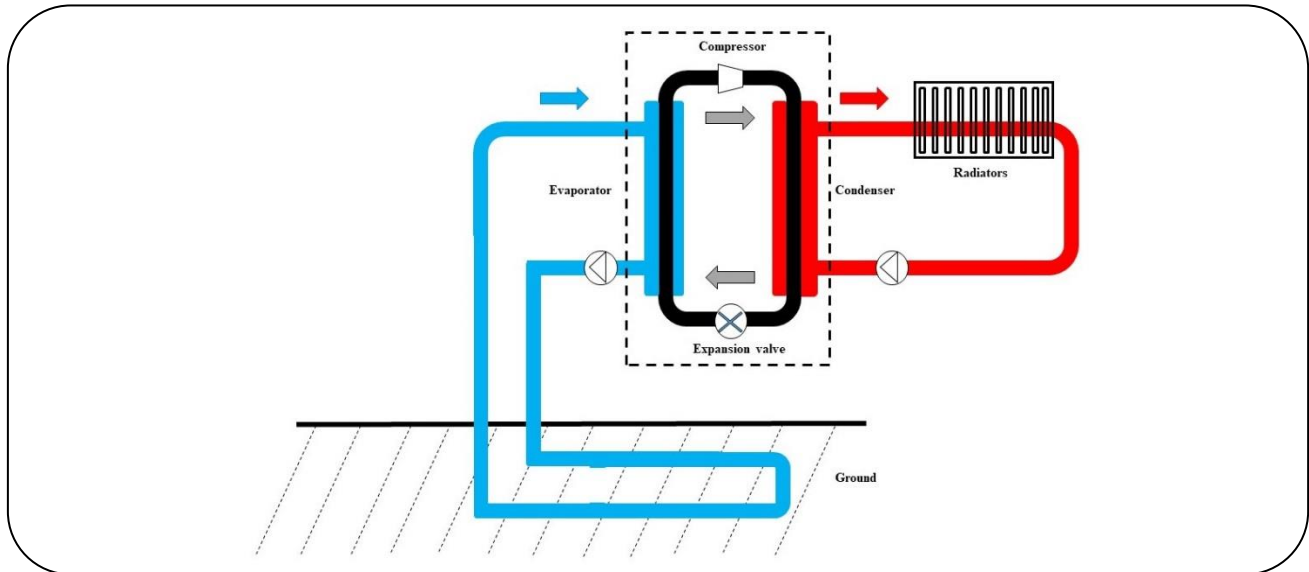


Fig. 1: Schematic view of HGHP.

Furthermore, regional climate data, along with other influential factors, were analyzed. The paper aims to meet the demand of decision-makers to develop policies focused on subsidizing the horizontal ground source systems. Finally, Iran's HGHP priority map will be accurately presented in this study to help policymakers with decisions concerning technology subsidization which helps the investigators to have a better picture of the total affecting parameters on GHP system installation.

EXPERIMENTAL SECTION

Modeling

The system was modeled for cooling and heating in a general steady-state, steady-flow process under normal conditions for simulated vapor-compression systems. R600a is considered the cycle refrigerant, a natural refrigerant with low environmental impact and excellent thermodynamic performance, with both evaporator and condenser are double-tube heat exchangers where the water and refrigerant move within the annulus and tube, respectively. The material for the ground heat exchanger was chosen to be polyethylene.

Refrigerant properties

Refrigerant properties are listed in Table 1 [27]:

Flow rates of refrigerant and water mass

Computation of properties for all the thermodynamic states is performed as given in Table 2:

The thermodynamic data required is obtained from reference [28].

Assuming zero rates of work crossing the boundaries of the control volume, mass flow rates of R600a both in the heating cycle ($\dot{m}_{R\cdot h}$) and cooling cycle ($\dot{m}_{R\cdot c}$) are computed by the first law of thermodynamic as follows:

$$\dot{m}_{R\cdot h} = Q_h / (h_{2\cdot h} - h_{3\cdot h}) \quad (1)$$

$$\dot{m}_{R\cdot c} = Q_c / (h_{1\cdot c} - h_{4\cdot c}) \quad (2)$$

Where Q_h (kW) and Q_c (kW) are the rate of the heat flow, which is transferred between the indoor water and refrigerant in the evaporator and condenser in the heating and cooling cycle.

The outdoor water mass flow rate in the heating cycle ($\dot{m}_{W\cdot h}$) and cooling cycle ($\dot{m}_{W\cdot c}$) is calculated through the following equations considering previous assumptions:

$$\dot{m}_{W\cdot h} = \frac{Q_{Eva\cdot h}}{c_{p\cdot W} \times (T_{W1\cdot h} - T_{W2\cdot h})} \quad (1)$$

$$\dot{m}_{W\cdot c} = \frac{Q_{Con\cdot c}}{c_{p\cdot W} \times (T_{W2\cdot c} - T_{W1\cdot c})} \quad (2)$$

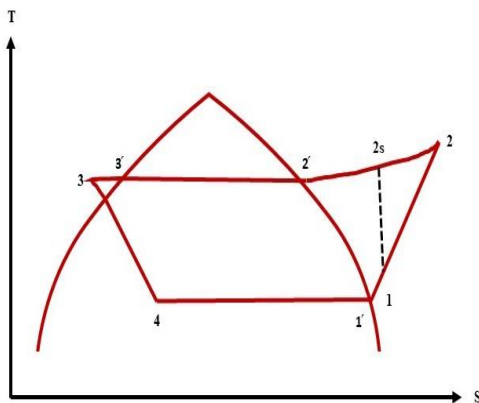
Where $Q_{Eva\cdot h}$ (kW) and $Q_{Con\cdot c}$ (kW) are the rates of heat flow between the refrigerant and groundwater water in heating and cooling cycles, respectively. In the previous equations, $T_{W1\cdot h}$ (°C), and $T_{W2\cdot h}$ (°C) are the HGHP inlet and outlet water temperatures in the heating cycle, and $T_{W1\cdot c}$ (°C) and $T_{W2\cdot c}$ (°C) are the HGHP inlet

Table 1: R600a properties.

Refrigerant	R600a (Isobutane)
Molecular weight	58.12
Normal boiling point (°C)	-11.7
Critical temperature (°C)	134.7
Critical pressure (kPa)	3640
ΔH_{vap} at 5 °C (kJ/kg)	350

Table 2: The thermodynamic calculation of states for R600a.

Input parameters	Output parameters
$T_1 = T_E + T_{superheating}, P_1 = P_E$	h_1 and s_1
$s_1 = s_{2s}, P_2 = P_c$ η_s, h_1, h_{2s} P_2, h_2	$h_2 = h_1 + \frac{h_{2s} - h_1}{\eta_s}$ s_2
$P_3 = P_2, T_3 = T_3 - T_{subcooling}$	s_3 and h_3
$T_4 = T_E, h_4 = h_3$	x_4 and s_4

**Fig. 2: T-S diagram for a heat pump.**

and outlet water temperatures in the cooling cycle, respectively. The thermodynamic properties of water flowing in the system are derived from the reference in the average temperature of GHX outlet and inlet both in heating and cooling cycles [29].

The length of the condenser and evaporator

Assuming R600a as the refrigerant goes into the internal tube and water flows through the external one counter-currently in a double-tube exchanger, the length of the evaporator (L_{Eva}) is calculated as follows [30]:

$$L_{Eva} = \frac{Q_{Eva} \cdot h}{\Delta T_{lm \cdot Eva} \cdot h} \times \left(\frac{1}{h_{R22 \cdot Eva} \cdot h \times \pi D_{I \cdot i \cdot Eva}} \right) \times \left(\frac{\ln(D_{I \cdot o \cdot Eva} / D_{I \cdot i \cdot Eva})}{2\pi \times K_{Eva}} \right) \times \left(\frac{1}{h_{W \cdot Eva} \cdot h \times \pi D_{I \cdot o \cdot Eva}} \right) \quad (3)$$

Where:

$\Delta T_{lm \cdot Eva} \cdot h$ is the Logarithmic Mean Temperature Difference (LMTD) of the evaporator in the heating cycle, $D_{I \cdot o \cdot Eva}$ (m) and $D_{I \cdot i \cdot Eva}$ (m) are the outer and inner diameters of the evaporator's inner tube,

K_{Eva} ($kW/(m^{\circ}C)$), is the thermal conductivity of the evaporator's inner tube and

$h_{R22 \cdot Eva} \cdot h$ ($kW/(m^2K)$) is the heat transfer coefficient of R600A in evaporator tube in heating cycle computed from Shah formula [30].

To describe the convection heat flow of circulating water in the evaporator in the heating cycle, the corresponding coefficient ($h_{W \cdot Eva} \cdot h$) can be defined by:

$$h_{W \cdot Eva} \cdot h = Nu_{w \cdot h} \times \frac{K_w}{D_{e \cdot Eva}} \quad (6)$$

Where:

K_w ($kW/(m^{\circ}C)$) is the thermal conductivity of water, $D_{e \cdot Eva}$ (m) is the equivalent diameter of the evaporator's outer tube and

$Nu_{w \cdot h}$ is the Nusselt number of source water in the heating cycle calculated utilizing Dittus–Bolter formula in turbulent conduit flow [30].

According to the previous assumptions, the condenser length is defined as follows:

$$L_{Con} = \frac{Q_{Con} \cdot c}{\Delta T_{lm \cdot Con} \cdot c} \times \left(\frac{1}{h_{R22 \cdot Con} \cdot c \times \pi D_{I \cdot i \cdot Con}} \right) \times \left(\frac{\ln(D_{I \cdot o \cdot Con} / D_{I \cdot i \cdot Con})}{2\pi \times K_{Con}} \right) \times \left(\frac{1}{h_{W \cdot Con} \cdot c \times \pi D_{I \cdot o \cdot Con}} \right) \quad (4)$$

Where:

$\Delta T_{lm \cdot Con} \cdot h$ is the LMTD of the condenser in the heating cycle,

$D_{I \cdot o \cdot Con}$ (m) and $D_{I \cdot i \cdot Con}$ (m) are the outer and inner diameters of the condenser's inner tube,

K_{Eva} ($kW/(m^{\circ}C)$) is the thermal conductivity of the condenser's inner tube and $h_{R22 \cdot Con} \cdot h$ ($kW/(m^2K)$) is the coefficient of condensation heat transfer for R600A in condenser tube in the cooling cycle calculated by Cavalini and Zenchin equation for forced convection condensation. The convection heat transfer coefficient of

flowing water in the condenser's outer tube in the cooling cycle ($h_{W\cdot Con\cdot c}$) is determined the same as that of the evaporator.

The GHX length

There are three basic types of outside loops for earth energy systems [31] and using a changed version of the CEES procedure [26].

For the reason that the ground temperature under the surface does not change significantly over the 12 months, in the Horizontal Heat Exchanger system, the temperature of the ground is calculated utilizing the average yearly temperature of soil on the surface (T_s). the methodology is as follows:

a) Choosing the rate of heat flow (Q_{GHX}) for heating ($Q_{Eva\cdot h}$) / cooling ($Q_{Con\cdot c}$) cycles,

b) Calculating the difference in temperature (ΔT) between the surface temperature (T_s) and the average value of inlet and outlet temperatures of water flowing in the ground exchanger

c) estimating the overall thermal resistance (R_{Total}) by:

$$R_{total} = R_w + R_p + R_s \quad (5)$$

Where:

R_w ($m^\circ C/kW$) is the resistance of the water flow:

$$R_w = \frac{1}{h_w \times \pi \times D_{i\cdot GHX} \times 2L_{GHX}} \quad (9)$$

R_p ($m^\circ C/kW$) is the resistance of the pipe wall.

$$R_p = \frac{\ln(D_{o\cdot GHX}/D_{i\cdot GHX})}{2\pi \times K_{p\cdot GHX} \times 2L_{GHX}} \quad (10)$$

R_s ($m^\circ C/kW$) is the thermal resistance of the soil.

$$R_s = \frac{F}{U_s \times (\pi \times D_{o\cdot GHX} \times 2L_{GHX})} \quad (6)$$

and:

h_w ($\frac{kW}{m^2K}$) is the water convection heat transfer coefficient in borehole pipe of GHX,

$D_{i\cdot GHX}$ (m) is GHX inner pipe diameter,

L_{GHX} (m) is length of GHX ,

$D_{o\cdot GHX}$ (m) is GHX outer pipe diameter and

$K_{p\cdot GHX}$ ($\frac{kW}{m^\circ C}$) is GHX pipe wall thermal conductivity;

F : Part-load factor of GHX, for heating and cooling cycles which is calculated from:

$$F_h = \frac{\tau_h}{T_h} \quad (7)$$

$$F_c = \frac{\tau_c}{T_c} \quad (8)$$

Power consumption in compressor and pump

Regarding the zero rates of work crossing the boundaries of the control volume, the compressor power consumptions for both heating and cooling cycles are calculated based on thermodynamics first law and :

$$W_{com\cdot c} = \dot{m}_{R\cdot c} \times \Delta h_{Com\cdot c} = \dot{m}_{R\cdot c} \times \frac{h_{2\cdot c} - h_{1\cdot c}}{\eta_{el\cdot c}} \quad (9)$$

$$W_{com\cdot h} = \dot{m}_{R\cdot h} \times \Delta h_{Com\cdot h} = \dot{m}_{R\cdot h} \times \frac{h_{2\cdot h} - h_{1\cdot h}}{\eta_{el\cdot h}} \quad (10)$$

For considering the losses in-ground heat exchanger, heat pump and an overestimate of 50% for losses in all fittings used, the required pumping head (H_{Pump}) could be obtained [30].

Consequently, the power of pumping (W_{Pump}) for heating and cooling cycles is estimated through the following equations:

$$W_{Pump\cdot h} = \dot{m}_{W\cdot h} \times H_{Pump\cdot h} / (\rho_{W\cdot h} \times \eta_{Pump\cdot h}) \quad (11)$$

$$W_{Pump\cdot c} = \dot{m}_{W\cdot c} \times H_{Pump\cdot c} / (\rho_{W\cdot c} \times \eta_{Pump\cdot c}) \quad (12)$$

In the end, for selecting the nominal power of the pump and compressor, the maximum power consumption in the heating and cooling cycle is chosen because it is not economically possible to procure two pumps and two compressors for all the circumstances; so the machine shall be able to meet the demands of both conditions.

$$W_{Com} = \text{Max} \{ W_{Com\cdot c} \cdot W_{Com\cdot h} \} \quad (13)$$

$$W_{Pump} = \text{Max} \{ W_{Pump\cdot h} \cdot W_{Pump\cdot c} \} \quad (14)$$

Economic modeling

The system should be modeled based on TYC, including capital and operating costs to be optimized by PSO. In this step, The TYC of the HGHP system is computed from:

$$TAC = C_{EL} + C_{Inv} \quad (20)$$

Where C_{EL} ($\$/y$) and C_{Inv} ($\$/y$) are the yearly expense of the electricity consumption and the initial investment for the system. The yearly electricity

consumption (E) can be achieved by adding the yearly electricity consumption of the pump and compressor as follows:

$$E = E_{Com} + E_{Pump} \quad (21)$$

$$E_{Com} = \tau \times \dot{m} \times \Delta h_{Com} = \tau \times \dot{m}_c \times (h_2 - h_1) \quad (22)$$

$$E_{Pump} = \frac{T \times \dot{V}_w \times H_{Pump}}{\eta_{Pump}} \quad (23)$$

$$C_{EL} = C_{El \cdot M} \times 12 \quad (24)$$

Where,

E_{Com} (kW h/y) is the compressor yearly energy consumption,

E_{Pump} (kW h/y) is the pump yearly energy consumption,

τ (h/y) is equivalent full-load hours,

t (h/y) is yearly operating hours,

\dot{V}_w (m^3/s) is volumetric flow rate of water in GHX and

$C_{El \cdot M}$ (\$/month) is the monthly power cost;

The monthly power cost may be estimated by multiplying the power price with power consumption in each month of the year. Iran's power price can be seen in Table 3.

C_{Inv} the yearly initial expense is calculated as follows:

$$C_{Inv} = (C_{Eva} + C_{Con} + C_{Com} + C_{Pump} + C_{GHX} + C_{AF}) \times CRF \quad (25)$$

CRF the capital recovery factor is computed from:

$$CRF = \frac{i}{1 - (i + 1)^{-n}} \quad (26)$$

Where:

i and n are annual interest and depreciation periods which are considered to be ten percent and ten years, respectively [26].

$$C_{Eva} = a1 \times A_{Eva}^{a2} \quad (27)$$

$$C_{Con} = a3 \times A_{Con}^{a4} \quad (28)$$

$$C_{Com} = a5 \times W_{Com}^{a6} \quad (29)$$

$$C_{Pump} = a7 \times W_{Pump}^{a8} \quad (30)$$

$$C_{GHX} = C_{Pipe} + C_{bore} = 2L_{GHX}C_{Pipe} + a9 \times L_{GHX} \quad (31)$$

Table 3: Iran's domestic power price [32].

Monthly power consumption (kWh)	Subsidized power price(cent)
0-100	1.36
100-200	1.85
200-300	3.94
300-400	5.44
400-500	6.89
500-600	8.20
600 >	11.1

Table 4: The values obtained for constants a1 to a9.

Constants	value
a1	499.1
a2	0.16
a3	748.6
a4	0.16
a5	233.3
a6	0.95
a7	308.9
a8	0.25 for a pump power of 0.02–0.3 kW 0.45 for a pump power of 0.3–20 kW 0.48 for a pump power of 20–200 kW
a9	10.4

Where C_{Eva} , C_{Con} , C_{Com} , C_{Pump} , C_{GHX} are the price of evaporator, condenser, pump, and GHX [33]. $a1$ to $a8$ are achieved by estimating the local cost of the apparatus or the surface area of the exchanger. $a9$ is calculated regarding the cost of digging the well-bores and burying the pipes underground. $a1$ to $a9$ are provided in Table 4 [25].

Furthermore, A_{Eva} and A_{Con} are the evaporator and the condenser of heat transfer surface areas, respectively. C_{AF} is the price of an antifreeze solution, which is estimated as follows:

$$C_{AF} = V_{Pipe \cdot in} \times c_{AF} \times VFA \quad (32)$$

Where:

$V_{Pipe \cdot in}$ (m^3) is pipe inside volume,

c_{AF} (\$/ m^3) is cost of antifreeze solution and VFA is volume fraction of antifreeze in the intermediate fluid;

Optimization by PSO

proposed initially by Eberhart and Kennedy in 1995, the PSO algorithm is a nature-inspired technique focused on the social behavior of bird flocking and fish schooling [34]. This approach is based on the particle swarm interaction [35] as a population-based stochastic optimization strategy using swarm intellects within the search space. Each molecule incorporates two-position and velocity values optimized during the iteration run by determining each particle's most significant experience (best position) and the leading achieved experience (worldwide position) of all particles.

The update of the particles' position and velocity must be processed through the following equations to satisfy the model constraints. The movement of each particle is related to the changes in its position and velocity.

$$P_i^{k+1} = P_i^k + V_i^{k+1} \quad (33)$$

where P_i^{k+1} and P_i^k are the position of particle i in the iteration $k+1$ and k , respectively, V_i^{k+1} is the particle's velocity in the $k+1$ iteration. A particle's velocity is defined as follows:

$$V_i^{k+1} = w \times V_i^k + c_1 \times \text{rand}_1 \times (Pbest_i - P_i^k) + c_2 \times \text{rand}_2 \times (Gbest_i - P_i^k) \quad (34)$$

Where $Pbest_i$ is the best so far the position of the particle i as the best experience, while $Gbest_i$ is the best position among the whole swarm with all the particles in movement as a global experience. c_1 and c_2 are the weighting components, while rand_1 and rand_2 are two random numbers between zero and one. The parameter w is the inertia component varying between w_{minimum} and w_{maximum} as illustrated in the following equation.

$$w = w_{\text{maximum}} - \frac{w_{\text{maximum}} - w_{\text{minimum}}}{\text{iter}_{\text{maximum}}} \times k \quad (35)$$

wk and $\text{iter}_{\text{maximum}}$ are the current iterations and the highest number of iteration during simulations, respectively. The overall steps of PSO towards solving an optimization are defined as shown in Table 5 [36]:

Moreover, the following constraints have to be applied in the model [25]:

- $\bar{T}_{\text{hour}\cdot c} - T_{\text{wi2}\cdot c} > 10 \text{ }^\circ\text{C}$: for assuring the proper heat exchange between the chilled water and the room space in the cooling cycle

- $T_{\text{wi2}\cdot h} - \bar{T}_{\text{hour}\cdot h} > 10 \text{ }^\circ\text{C}$: for assuring the proper

Table 5: PSO overall steps.

Step	Description
1	Setting w_{maximum} , w_{minimum} , c_1 and c_2
2	Generation of the initial population with P and V
3	$K=1$
4	Calculation of Fitness, find the best answer
5	$Pbest_i^k = P_i^k$ and $Gbest_i^k = P_b^k$
6	$w = w_{\text{maximum}} - \frac{w_{\text{maximum}} - w_{\text{minimum}}}{\text{iter}_{\text{maximum}}} \times k$
7	$V_i^{k+1} = w \times V_i^k + c_1 \times \text{rand}_1 \times (Pbest_i - P_i^k) + c_2 \times \text{rand}_2 \times (Gbest_i - P_i^k)$ $P_i^{k+1} = P_i^k + V_i^{k+1}$ Calculation of Fitness
8	Updating $Pbest$
9	Updating $Gbest$
10	If $K = \text{iter}_{\text{maximum}} \rightarrow$ End ($Gbest_i^k$ is the answer) Else $K = K+1$ and going to Step 5

heat exchange between the hot water and the room space in the heating cycle

- $T_{\text{wi1}\cdot c} - T_{\text{Eva}\cdot c} > 10 \text{ }^\circ\text{C}$: for assuring the proper heat exchange between the chilled water and the refrigerant in the evaporator in the cooling cycle

- $T_{\text{Con}\cdot h} - T_{\text{wi1}\cdot h} > 10 \text{ }^\circ\text{C}$: for assuring the proper heat exchange between the hot water and the refrigerant in the condenser in the heating cycle.

Model validation

The modeling and optimizing method should be validated by checking the results with those published in previous studies [26]. Consequently, 7 climatic regions were considered based on the reference as follows:

- Regions one to three; denote the cold climate.
- Region four; represents the mild climate.
- Regions five to seven; indicate the hot climate.

For comparing the numerical results for different regions, the total cooling, and heating loads were regarded as equivalent to 36 kW, and the total operation time for cooling and heating cycles was regarded as equivalent to 2700 hours each year. A set of optimization input factors, including specification of the soil, system operation conditions, and the equipment specifications,

Table 6: Soil and equipment specifications.

$K_s = 2.4 \text{ W}/(\text{m}^2 \cdot ^\circ\text{C})$	$T_s = 16^\circ\text{C}$
$U_s = 12 \text{ W}/(\text{m}^2 \cdot ^\circ\text{C})$	$\eta_s = 75\%$
$\eta_{el} = 80\%$	$\eta_{\text{pump}} = 80\%$
$\eta_M = 80\%$	$K_{\text{Con}} = 0.398 \text{ kW}/(\text{m}^2 \cdot ^\circ\text{C})$
$K_{\text{p-GHX}} = 0.39979 \text{ kW}/(\text{m}^2 \cdot ^\circ\text{C})$	$K_{\text{Eva}} = 0.398 \text{ kW}/(\text{m}^2 \cdot ^\circ\text{C})$
$D_{\text{I-o-Con}} = 0.0348$	$D_{\text{I-i-Con}} = 0.0318$
$D_{\text{I-o-Eva}} = 0.0348$	$D_{\text{I-i-Eva}} = 0.0318$

Table 7: The specifications of seven regions to validate the modeling and optimizing method.

Region	T_c	T_h	τ_c	τ_h	Q_c	Q_h	T_s
1	300	2400	120	960	4	32	10
2	540	2160	216	864	7.2	28.8	13
3	900	1800	360	720	12	24	16
4	1350	1350	540	540	18	18	19
5	1800	900	720	360	24	12	22
6	2160	540	846	216	28.8	7.2	25
7	2400	300	960	120	32	4	28

are regarded identical in 7 regions (Table 6). The properties of all the regions and numerical results can be seen in Table 7 and Table 8.

As shown in Table 8, the deviation between reference and results of this study is negligible as proof of model validation. The influence of regional factors, including heating and cooling load, cooling to heating thermal load ratio (Q_c/Q_h), and the soil heat transfer coefficient (U_s) on TYC, should be studied to render a better picture in general exploration. The numerical outcomes are shown in Fig. 3, Fig. 4, and Fig. 5.

Results from Fig. 3 show that optimized TYC increases by changing the HGHP system cooling and heating loads basically because the total cost, including operating and initial investment, grows. Also, the effect of cooling to

heating thermal load ratio (Q_c/Q_h) on TYC is significant in Fig. 4. It is understood that the total yearly cost is considerably lower in mild climates ($Q_c/Q_h \sim 1$) than that of hot areas ($Q_c/Q_h > 1$) and cold climates ($Q_c/Q_h < 1$). Furthermore, it can be concluded that TYC is greater in cold regions than that in hot regions. To put it another way, TYC is higher in cold regions than hot ones that are higher than temperate regions, which could be considered the fundamental parameter in making an HGHP potential map based on economic factors. From Fig. 5, it can be understood that TYC value grows gently by growth in soil heat transfer coefficient. Furthermore, dry loam-type soil has the highest amount of TYC. To put it another way, the soil's class and wetness is the second major factor for SGE potential appraisal.

RESULTS AND DISCUSSION

Ninety-six cities of Iran are chosen based on which the model and optimization are carried out. These cities are selected in a way that the required data is available and authentic [37].

Calculation of cooling and heating load

calculated the cooling and heating load, three ordinary buildings with an overall area of 70m², 96m², and 110 m² are simulated as the majorly permitted class of justly built or constructing apartments in the country [38]. The specification of material used hypothetically in three buildings is chosen regarding the local standards [39] to guarantee the building standard energy performance. The data is listed in Table 9.

Energy Plus used in this study utilizes building physics for air, humidity, and heat transfer, including the separate treatment of radiative and convective heat transfer to promote radiant device modeling and thermal comfort metric calculation; calculates light, shade, and visual comfort metrics; supports modular component-level configuration of HVAC, refrigeration systems, and plant [40]. Energy Plus software computes cooling and heating load numbers, which are essential to keep the environmental condition for human living in comfort that ranges almost from 19 °C to 28 °C based on the standard [41]. The heating and cooling loads to be modeled and optimized are considered the average amount of three buildings.

Table 8: Optimized TYC values for assumed regions [26].

	1	2	3	4	5	6	7
Results by GA (\$/y) in reference	3224.3	1931.0	901.7	619.3	713.2	865.2	1101.6
Results by NM (\$/y) in reference	3216.5	1931.1	901.3	617.5	712.5	864.3	1100.7
Calculated results (\$/y)	3220.0	1930.0	900.5	619.4	714.7	864.0	1100.2

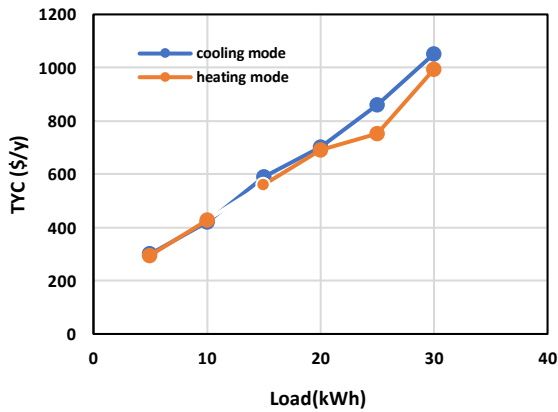


Fig. 3: Effect of cooling (Q_c) and heating (Q_h) load on TYC

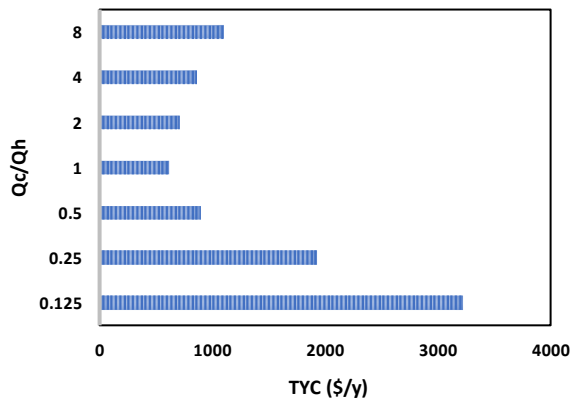


Fig. 4: Change in the optimized TYC with cooling to heating thermal load ratio (Q_c/Q_h).

Computation of operation hours

Early operating hours mean the calculated hours each year, which the HGHP is needed to run for keeping comfortable conditions in the buildings. The operation hours are calculated separately for cooling and heating mode; times in which the building temperature is higher than the comfortable temperature is considered as cooling mode and the time in which the building temperature is under the comfortable temperature is considered as heating mode. The following equations can estimate yearly operating hours in heating and cooling cycles:

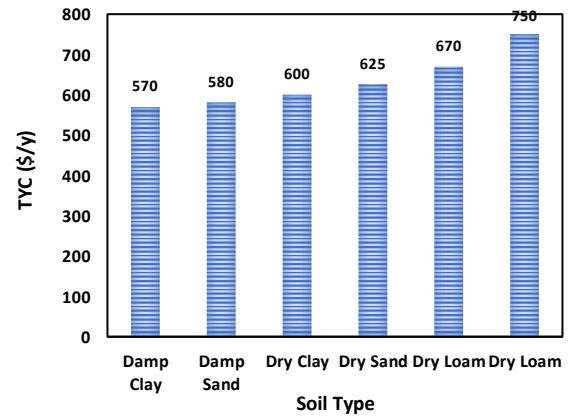


Fig. 5: Change in the optimized TYC value with the type of soil [26].

$$t_c = \sum_{n=1}^{total\ year\ hours} \bar{T}_{hour} - T_{Comfort.c} \quad (36)$$

$$IF \bar{T}_{hour} > T_{Comfort.c}$$

$$t_h = \sum_{n=1}^{total\ year\ hours} T_{Comfort.h} - \bar{T}_{hour} \quad (37)$$

$$IF \bar{T}_{hour} < T_{Comfort.h}$$

Where:

t_c/t_h (h/y) : Yearly operating hours in cooling/heating cycles

\bar{T}_{hour} (°C) : Air average temperature

$T_{Comfort.c}$ (°C) : Comforting temperature in the cooling cycle

$T_{Comfort.h}$ (°C) : Comforting temperature in the heating cycle

Equivalent full load hours (τ) represent the overall hours that the HGHP should run in full capacity to meet the heating & cooling demand, which is computed by the following equations:

$$\tau_c = \sum_{n=1}^{total\ year\ hours} \frac{\bar{T}_{hour} - T_{Comfort.c}}{T_{db.c} - T_{Comfort.c}} \quad (38)$$

$$IF \bar{T}_{hour} > T_{Comfort.c}$$

Table 9: Building material specifications.

Item	Thickness(m)	U (W/m ² .K)
Exterior wall	0.27	1.78
Interior wall	0.12	2.31
Exterior roof	0.34	0.32
Interior roof	0.33	0.33
Window	-	3.23
Exterior door	0.13	3.92
Interior door	0.10	3.97

Table 10: Required and estimated data for spatial exploration; 96 cities of Iran.

City	Province	SDB	WDB	Tair	Ts	tc	th	toc	toh	Qc	Qh
Ahvaz	Khuzestan	46.4	3.3	26	27.3	750	2310	181.4	1176.5	12.1	8.4
Abadan	Khuzestan	45.6	2.8	25.9	27.6	390	3030	67.2	1700.4	11.8	8.5
Shoshtar	Khuzestan	45.8	2.2	24.1	26.21	900	1770	194.3	742.2	11.7	8.8
Tabas	Yazd	44.4	-2.2	18.1	21	690	1620	144.4	372.4	11.6	11.1
Gheshm	Hormozgan	41.4	13.6	30.6	31.96	900	1920	267.4	1209.8	11.4	3.6
Bandarabbas	Hormozgan	40.6	7.5	27	29.2	420	2790	84.7	1803.3	10.9	6.1
Bushehr	Bushehr	40	5.8	26.5	26.7	690	2400	213.2	1264.6	10.5	7.2
Gachsaran	Kohkiloye va Boyerahmad	42.5	-0.3	22	25.1	780	2430	218.2	893.1	10.3	10.3
Genaveh	Bushehr	38.1	5.3	25.4	27.5	570	2820	212.4	1669	10.1	7.4
Kazeroon	Fars	43.1	-0.3	22.5	25.8	930	1440	244.8	373.4	10	10.2
Bastak	Hormozgan	42.5	3.3	27.4	30.05	930	1530	246.9	549.3	9.7	8.2
Bafgh	Yazd	40.6	-4.4	16.6	19.7	360	3180	65.9	1369.9	9.7	12
Yazd	Yazd	40	-5.3	18.8	18.9	1170	630	336.6	73.2	9.5	12.5
Semnan	Semnan	38.3	-4.4	14.3	17.2	570	2880	213.9	1213	9.4	12
Fasa	Fars	39.4	-1.7	19.6	23.44	300	3480	58	2053	9.2	10.7
Jahrom	Fars	41.4	-2.2	21.8	25.5	600	2340	140.6	677.2	9.2	11.2
Izeh	Khuzestan	41.1	1.4	19.6	23.1	840	1650	248.4	658.4	9.1	9.2
Qom	Qom	40	-4.4	13.4	16.3	270	3510	51.9	2024.2	9.1	12.1
Saveh	Markazi	39.2	-4.4	8.9	15.42	630	2670	210.4	1052.6	8.9	12.1
Torbat jam	Khorasane Razavi	36.7	-11.4	14.4	17.6	180	3540	57.2	1687.6	8.8	15.3
Baghmalek	Khuzestan	39.4	2.5	21.7	25.14	840	2250	252.7	768.6	8.8	8.9
Aghghola	Golestan	37.2	-2.8	17	20.1	300	3270	71.3	1543.9	8.6	11.1
Garmsar	Semnan	38.9	-6.4	13.1	15.7	570	2910	199.9	1173.6	8.6	12.9
FiroozAbad	Fars	38.1	-2.8	23.1	26.8	780	2160	259.8	596.8	8.5	11.1
Tehran	Tehran	37.8	-4.4	17.2	15.3	450	2790	123	959.2	8.5	11.9

Table 11: Required and estimated data for spatial exploration; 96 cities of Iran. (Continuation)

BoyerAhmad	Kohkiloye va Boyerahmad	34.4	-9.7	17.5	20.5	390	3300	168.4	1461.6	8.4	14.5
Ardestan	Esfahan	38.9	-5.6	15.4	18	300	3510	58.7	1894	8.3	12.5
Gorgan	Golestan	35	-0.8	14.9	17.9	690	2070	291.3	848.4	8.3	10.3
Kalaleh	Golestan	37.5	-6.7	13.7	16.65	300	3360	65.9	1476.6	8.3	13.1
Shiraz	Fars	38.1	-3.3	17.5	21.9	360	2940	104.4	1012.7	8.2	11.5
Khaf	Khorasane Razavi	36.1	-11.1	15.4	18.62	720	1560	193.8	173.1	8.2	15.2
Ferdos	Khorasane Razavi	37.8	-8.3	16.8	19.86	720	2460	240.8	601.3	8.1	13.8
Poldokhtar	Lorestan	38.3	-4.7	19.2	21.91	300	3480	62.4	1903.1	8	12.1
Zahedan	Sistano Balochestan	37.5	-6.9	18.2	22.9	570	2760	218.4	996.9	8	13.1
Rey	Tehran	38.1	-5.8	16.1	15.3	210	3540	50	1946.4	8	12.7
Dargaz	Khorasane Razavi	36.4	-9.2	15.1	18.2	630	2730	230.2	862	7.9	14.3
Varamin	Tehran	38.1	-7.2	16.8	15.37	840	2010	294.9	405.5	7.9	13.3
Esfahan	Esfahan	36.4	-6.1	16.2	16.4	930	1050	353.1	160.6	7.8	12.7
Naeen	Esfahan	36.9	-6.9	15.8	18.6	300	3270	73.5	1301.5	7.8	13.1
Zarand	Kerman	36.7	-8.6	16.2	19.98	570	3030	215.5	1186.6	7.8	14
KhoramAbad	Lorestan	39.2	-6.4	15.3	17.8	300	3390	63.1	1653.4	7.8	13
Pakdasht	Tehran	36.1	-5.3	17.5	15.24	570	2790	233.2	1032.3	7.8	12.4
Azadshahr	Golestan	35.6	-2.5	13.2	16.43	600	2730	215.5	1219.3	7.6	11
Shahrood	Semnan	35	-8.6	14.4	17.9	570	3060	216.7	1159.4	7.6	14
Kerman	Kerman	36.4	-11.4	17.2	19.7	780	720	224.9	46.6	7.5	15.3
Delijan	Markazi	37.5	-11.4	16	16.54	300	3450	62.5	1435.7	7.5	15.3
Pars-Abad	Ardabil	35.3	-5.8	11.3	13.2	540	1710	172.1	241.5	7.4	12.7
Mashhad	Khorasane Razavi	35.3	-9.4	13.8	16.8	540	1710	172.1	211.2	7.4	14.4
Neka	Mazandaran	33.6	-1.7	15.6	17.81	510	2940	209.1	1321.5	7.2	10.7
BooienZahra	Qazvin	36.4	-12.2	11.4	15.38	240	3420	60.1	1347.9	7.2	15.9
Karaj	Alborz	35.6	-8.3	12.3	14.9	180	3540	55.7	1758.1	7.1	13.8
Lenjan	Esfahan	35	-6.7	14.4	15.64	180	3540	55.4	1797.9	7.1	13
Mobarakeh	Esfahan	35	-6.7	14.8	15.56	570	2910	230.4	1097.8	7.1	13
Arak	Markazi	35.6	-12.2	11.4	15.07	900	1080	336.1	117.5	7.1	15.9
Qazvin	Qazvin	35.3	-10.6	12.4	14.88	900	1080	348.6	124.1	7.1	14.9
Lordegan	Shahrkord	36.7	-6.9	16.2	19.7	300	3390	71.1	1523.1	7.1	13.1
Sanandaj	Kordestan	36.9	-13.1	11.2	13.3	360	2910	85	784.7	7	16.5
Bojnord	N_Khorasan	35	-12.5	13.2	16.3	180	3540	53.8	1600.6	7	15.8
Sari	Mazandaran	33.6	-3.1	14.6	17.5	420	1500	135.3	210.5	6.9	11.4
Takestan	Qazvin	35.3	-11.7	11.8	15.3	900	1080	348.6	119.6	6.9	15.5

Table 12: Required and estimated data for spatial exploration; 96 cities of Iran. (Continuation)

Zanjan	Zanjan	33.1	-16.7	11.2	11.9	480	960	158.1	60	6.9	17.8
Tabriz	E_Azarbayjan	33.9	-10.8	12.3	10.6	900	990	371	101.7	6.8	15
Rasht	Gilan	31.9	-2.2	12.5	17.59	90	3600	27.5	2121.7	6.8	11.1
Malayer	Hamedan	35	-11.7	12.3	14.65	570	3000	224.6	928.9	6.8	15.5
Baft	Kerman	33.1	-8.3	16.3	20	570	570	154.1	26.7	6.7	13.8
Ilam	Ilam	35	-4.4	20	22.7	180	3540	56.7	1844.4	6.6	12
Ivan	Ilam	35	-4.4	19.7	22.3	570	2820	232.5	1140.4	6.6	12
Behshahr	Mazandaran	33.3	-2.2	16.6	18.26	150	3720	35.8	2406.1	6.6	11
Nahavand	Hamadan	35.8	-11.7	12.6	14.83	1290	480	497.4	24.4	6.5	15.5
Kermanshah	Kermanshah	36.4	-10	14	15.8	1290	480	465.3	25.8	6.3	14.7
Farsan	Chahar mahale Bakhtiyari	35	-14.2	14.6	18.11	570	2460	257.5	579	6.2	16.8
Bonab	E_Azarbayjan	34.4	-10.3	10.1	12.1	150	3690	38.8	2063.3	6.2	14.8
W-EslamAbad	Kermanshah	35.6	-8.3	17.4	19.62	330	3030	102.9	1208.9	6.2	13.8
Talesh	Gilan	30.6	-1.7	9.9	12.49	30	3780	5.4	2415.5	6.1	10.6
Lahijan	Gilan	31.4	-0.6	14.8	17.7	390	2790	173.9	1053.1	6.1	10.2
MiandoAb	W_Azarbayjan	33.9	-11.7	9.7	12.65	660	2130	279.4	353.6	6	15.5
Songhor	Kermanshah	35.6	-16.1	12.6	14.55	600	2760	221.6	628.8	5.9	17.6
Natanz	Esfahan	33.9	-7.8	19.7	17.5	480	1800	157.2	245.5	5.7	13.5
Tooyserkan	Hamedan	34.4	-16.9	12.2	14.2	360	2610	116.9	446.1	5.7	18
kangavar	Kermanshah	35	-4.2	12.4	14.35	210	2970	72.1	1394.8	5.6	11.9
Bijar	Kurdestan	32.5	-16.1	9.6	10.86	390	3000	164.7	735.8	5.6	17.6
Bookan	W-Azarbayjan	34.2	-15.3	11.2	13.8	510	2850	216.8	784.6	5.6	17.1
ShahreKord	Chahar Mahale Bakhtiyari	33.3	-14.2	13.9	16.7	150	3570	38	1572.3	5.5	16.8
Hamedan	Hamedan	33.9	-16.4	12.3	14.8	840	1170	349.3	113.3	5.5	17.7
Sahneh	Kermanshah	35	-4.2	12.9	14.79	270	3300	64.2	1514.7	5.5	11.9
Dorood	Lorestan	33.3	-17.5	13.2	15.8	390	3180	167	1043.1	5.3	18.1
Boroojen	Shahrkord	33.1	-13.6	14	16.8	150	3570	34.8	1375	5.2	16.4
Urmia	W-Azarbayjan	31.1	-11.9	11.5	12	300	3180	139.5	1154.1	5.2	15.6
Savadkooh	Mazandaran	33.1	-12.2	12.3	16.79	150	3480	40	1203.5	5.1	15.9
Semirom	Esfahan	30.6	-11.9	14.7	17.36	300	3210	139.4	1121.9	4.8	5.9
Damghan	Semnan	30	-18.1	14.1	16.49	150	1080	42.3	49.7	4.8	18.4
Ahar	E-Azarbayjan	31.1	-13.6	9.3	10.9	660	780	298.1	50	4.6	16.4
Azna	Lorestan	31.9	-19.4	13	15.84	420	2700	207	472.2	4.6	18.9
Meshginshahr	Ardabil	30.3	-17.8	8.7	10.99	30	3810	2.4	1491	4.5	18.2
Kalibar	E-Azarbayjan	31.1	-13.6	9.6	11.58	390	2760	192.1	600.3	4.4	16.4
Sarab	E-Azarbayjan	30.6	-16.7	8.5	10.19	30	3780	5.4	1532.4	4.1	17.8

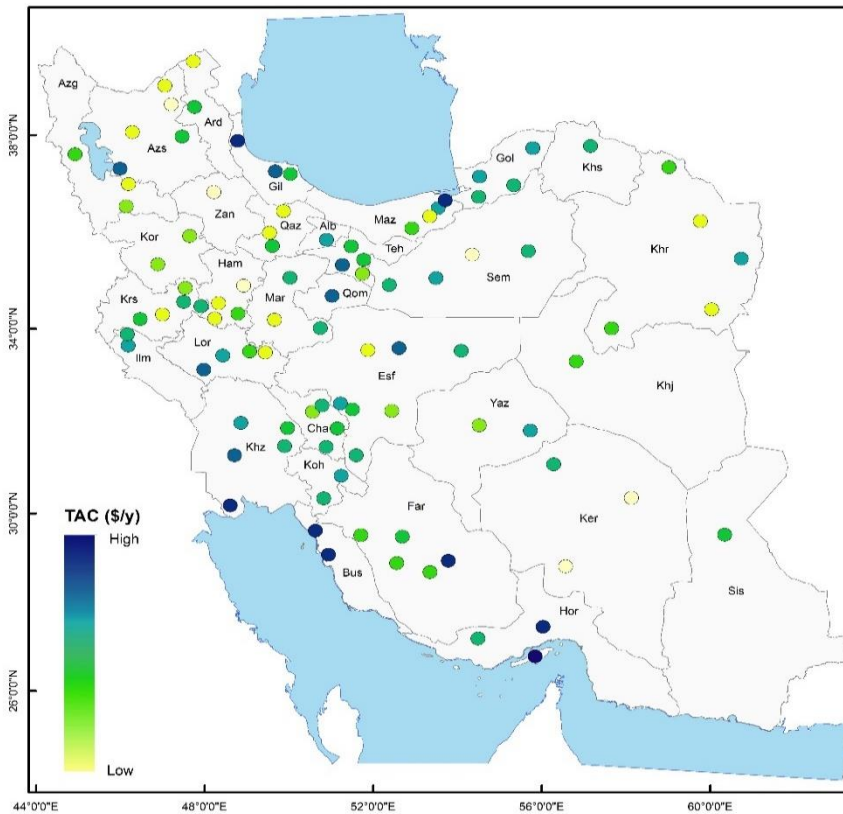


Fig. 6: Iran's potential map for HGHP implementation based on economic factors.

$$\tau_h = \sum_{n=1}^{\text{total year hours}} \frac{T_{\text{Comfort.c}} - \bar{T}_{\text{hour}}}{T_{\text{Comfort.c}} - T_{\text{db.h}}} \quad (39)$$

IF $\bar{T}_{\text{hour}} < T_{\text{Comfort.h}}$

Where,

$T_{\text{db.c}}$ ($^{\circ}\text{C}$): design dry temperature in the cooling cycle

$T_{\text{db.h}}$ ($^{\circ}\text{C}$): design dry temperature in the heating cycle

After all, data required for the final spatial exploration can be found in Table 10 for every 96 cities in Iran.

Spatial exploration

The modeling and optimization method described in the paper is carried out for 96 regions of Iran, for which the TYC numbers are calculated. The value of TYC varies from 917.1 \$/y to 1436.4.4 \$/y and from light red (the best region from an economic perspective) to dark blue (the worst region from an economic point of view) in color illustrated in Fig. 6.

This HGHP potential map highlights convenient regions

for utilization of horizontal geothermal heat pumps, supporting governmental and private organizations for policies regarding subsidization and funding strategies.

CONCLUSIONS

HGHP system utilization was investigated economically, and different involving significant factors such as climatic and geological parameters were studied to find the best TYC as the primary objective function between 96 cities of Iran. The country horizontal shallow geothermal mapping was presented, supporting governmental and private organizations regarding subsidization and funding strategies. Furthermore, the thermos-economic tools used in this paper, including HGHP modeling, PSO methodology, heating/cooling load estimation of exploration, apartments in comfortable conditions, and regional can be utilized in all the other regions. The novel studies may be improved with more precise estimates by implementing higher accuracy inputs on climate and geological data. It

is also recommended to investigate many cities to have a detailed and accurate priority map.

Nomenclature

η_s	Isentropic efficiency of compressor, %
η_{el}	Electric efficiency of compressor, %
η_{pump}	Electric efficiency of circulating pump, %
η_M	Efficiency of pump motor, %
μ	Dynamic viscosity, Pa.s
ΔP	Pressure drop of water flow, Pa
τ	System full capacity operating hours
GA	Genetic algorithm optimization technique
VGHE	Vertical ground heat exchanger
A	Heat transfer surface area of exchanger, m ²
a_1 - a_9	Constants in computing the equipment cost
c_{AF}	Cost of anti-freeze solution, \$/m ³
C_{El}	Annual cost of power consumption, \$/y
C_{Inv}	Initial or investment cost per operating years of the system, \$/y
c_p	Specific heat, kJ/kg °C
c_{pipe}	Cost of polyethylene pipe, \$/m
COP	Coefficient of performance
CRF	Capital recovery factor
$D_{e,EVA}$	Equivalent diameter of the evaporator annulus, m
D_{GHX}	GHX nominal pipe diameter, in
$D_{i,GHX}$	GHX inner pipe diameter, m
$D_{o,GHX}$	GHX outer pipe diameter, m
$D_{I,I,Con}$	Inner diameter of condenser's inner pipe, m
$D_{I,I,Eva}$	Inner diameter of evaporator's inner pipe, m
$D_{I,O,Con}$	Outer diameter of condenser's inner pipe, m
$D_{I,o,Eva}$	Outer diameter of evaporator's inner pipe, m
E	Annual power consumption, kW h/y
F	Part-load factor
h	Enthalpy, kJ/kg
J	Convection heat transfer coefficient, kW/(m ² K)
H_{Pump}	Pump head, m
i	Interest Rate, %
K_{Con}	Thermal conductivity of inner pipe of condenser, kW/(m °C)
K_{eva}	Thermal conductivity of inner pipe of evaporator, kW/(m °C)
$K_{p,GHX}$	Thermal conductivity of GHX pipe, kW/(m °C)
K_w	Water thermal conductivity, kW/(m °C)
L	Length of heat exchanger, m
\dot{m}	Mass flow rate, kg/s
n	Depreciation time, y

Nu	Nusselt number
Q	Thermal load, kW
R	Effective thermal resistance, °C/kW
RH	Relative humidity, %
t	Annual operating hours, h/y
\bar{T}_{Air}	Annual average air temperature, °C
T_{Con}	Condensation temperature, °C
T_{Eva}	Evaporation temperature, °C
T_s	Annual average soil temperature, °C
$\bar{T}_{Surface}$	Annual average soil surface temperature, °C
$T_{superheating}$	Superheating temperature, °C
$T_{subcooling}$	Sub cooling temperature, °C
$T_{comfort}$	Comfortable temperature, °C
T_{db}	Design dry bulb, °C
T_{wb}	Wet bulb temperature, °C
T_{w1}	Water temperature at the inlet of heat pump, °C
T_{w2}	Water temperature at the outlet of heat pump, °C
T_{wi1}	Building circulating water temperature at the inlet of heat pump, °C
T_{wi2}	Building circulating water temperature at the inlet of heat pump, °C
TAC	Total annual cost, \$/y
U	Heat transfer coefficient, kW/m ² K
$V_{pipe,in}$	Pipe inside volume, m ³
VFA	Volume fraction of the anti-freeze in the intermediate fluid, %
W	Power consumption, kW
AF	Anti-freeze
b	Borehole of GHX
c	Cooling mode
Con	Condenser
Con	Compressor
Eva	Evaporator
GHX	Ground heat exchanger
h	Heating mode
HP	Heat pump
i	Inner
M	Monthly
Min	Minimum
Max	Maximum
o	Outer
Pump	Circulating pump
R	Refrigerant
S	Soil
VFA	Volume fraction of anti-freeze
W	Water

Received : Jul. 23, 2021 ; Accepted : Nov. 29, 2021

REFERENCES

- [1] Rogelj J., Huppmann D., Krey V., Riahi K., Clarke L., Gidden M., Nichollas Z., Meinshausen M., [A New Scenario Logic for the Paris Agreement Long-Term Temperature Goal](#), *Nature*, **573(7774)**: 357-363 (2019).
- [2] Rahmani O., Rezania S., Beiranvandpour A., Aminpour S., [An Overview of Household Energy Consumption and Carbon Dioxide Emissions in Iran](#), *Processes*, **8(8)**: 994 (2020).
- [3] Rhodes Christopher J., [The 2015 Paris Climate Change Conference: COP21 \[J\]](#), *Science Progress*, **99(1)**: 97-104 (2016).
- [4] Deng Y., [Impact of Ventilation Rates on Indoor Thermal Comfort and Energy Efficiency of Ground-Source Heat Pump System](#), *Sustainable Cities and Society*, **37**: 154-163 (2018).
- [5] Bastani A., Eslamnejad P., Nguyen A., [Experimental Characterization of a Transcritical CO₂ Direct Expansion Ground Source Heat Pump for Heating Applications](#), *Energy and Buildings*, **212**: 109828 (2020).
- [6] Atam E., Helsen L., [Ground-Coupled Heat Pumps: Part 2—Literature Review and Research Challenges in Optimal Design](#), *Renewable and Sustainable Energy Reviews*, **54**: 1668-1684 (2016).
- [7] Seo Y., Seo U.-J., [Ground Source Heat Pump \(GSHP\) Systems for Horticulture Greenhouses Adjacent to Highway Interchanges: A Case Study in South Korea](#), *Renewable and Sustainable Energy Reviews*, **135**: 110194 (2021).
- [8] Mohammadzadeh Bina S., Fujii H., Tsuya S., Kosukegawa H., Naganawa S., Harada R., [Evaluation of Utilizing Horizontal Directional Drilling Technology for Ground Source Heat Pumps](#), *Geothermics*, **85**: 101769 (2020).
- [9] Alshehri F., Beck S., Ingham D., Ma L., Pourkashanian M., [Techno-Economic Analysis of Ground and Air Source Heat Pumps in Hot Dry Climates](#), *Journal of Building Engineering*, **26**: 100825 (2019).
- [10] Lim T.H., [Geothermal Heat Pump System for US Residential Houses: Barriers of Implementation and It's Environmental and Economic Benefits](#), MSc Thesis, University of Michigan (2014).
- [11] Duffield W.A., Sass J.H., [“Geothermal Energy, Clean Power from the Earth's Heat: Usgs Circular 1249, in US Department of the Interior”](#), US Geological Survey. (2003).
- [12] Aditya G.R., Narsilio G.A., [Environmental Assessment of Hybrid Ground Source Heat Pump Systems](#), *Geothermics*, **87**: 101868 (2020).
- [13] Karytsas S., Choropanitis I., [Barriers Against and Actions Towards Renewable Energy Technologies Diffusion: A Principal Component Analysis for Residential Ground Source Heat Pump \(GSHP\) Systems](#), *Renewable and Sustainable Energy Reviews*, **78**: 252-271 (2017).
- [14] Somogyi V., Sebestyén V., Nagy G., [Scientific Achievements and Regulation of Shallow Geothermal Systems in Six European Countries – A Review](#), *Renewable and Sustainable Energy Reviews*, **68**: 934-952 (2017).
- [15] Ondreka J., Rusgen H., Stober I., Czurda K., [GIS-Supported Mapping of Shallow Geothermal Potential of Representative Areas in South-Western Germany—Possibilities And Limitations](#), *Renewable Energy*, **32(13)**: 2186-2200 (2007).
- [16] Galgaro A., Di Sipio E., Teza G., Destro E., [Empirical Modeling of Maps of Geo-Exchange Potential for Shallow Geothermal Energy at Regional Scale](#), *Geothermics*, **57**: 173-184 (2015).
- [17] Nam Y., Ooka R., [Development of Potential Map for Ground and Groundwater Heat Pump Systems and the Application to Tokyo](#), *Energy and Buildings*, **43(2)**: 677-685 (2011).
- [18] Blum P., Campillo G., Kölbl T., [Techno-Economic and Spatial Analysis of Vertical Ground Source Heat Pump Systems in Germany](#), *Energy*, **36(5)**: 3002-3011 ().
- [19] Alcaraz, M., Garcia_Gil, A., Vazquez_Sune, E., [Use Rights Markets for Shallow Geothermal Energy Management](#), *Applied Energy*, **172**: 34-46 (2016).
- [20] Gemelli A., Mancini A., Longhi S., [GIS-Based Energy-Economic Model of Low Temperature Geothermal Resources: A Case Study in the Italian Marche Region](#), *Renewable Energy*, **36(9)**: 2474-2483 (2011).
- [21] Sivasakthivel T., Murugesan K., Thomas H.R., [Optimization of Operating Parameters of Ground Source Heat Pump System for Space Heating and Cooling by Taguchi Method and Utility Concept](#), *Applied Energy*, **116**: 76-85 (2014).

- [22] Robert F., Gosselin L., **New Methodology to Design Ground Coupled Heat Pump Systems Based on Total Cost Minimization**, *Applied Thermal Engineering*, **62(2)**: 481-491 (2014).
- [23] Sáez Blázquez C., Borge-Deiz D., Martin Nieto I., Farfan Martin A., Gonzalez-Aguilera D., **Technical Optimization of the Energy Supply In Geothermal Heat Pumps**. *Geothermics*, **81**: 133-142 (2019).
- [24] Cui Y., Jie Z., Ssenoga T., Junze C., Hongyu B., Xiangjie C., Stamatis Z., Soleimani Z., **Techno-Economic Assessment of the Horizontal Geothermal Heat Pump Systems: A Comprehensive Review**, *Energy Conversion and Management*, **191**: 208-236 (2019).
- [25] Sanaye S., Niroomand B., **Thermal-Economic Modeling and Optimization of Vertical Ground-Coupled Heat Pump**, *Energy Conversion and Management*, **50(4)**: 1136-1147 (2009).
- [26] Sanaye, S. and B. Niroomand, **Horizontal Ground Coupled Heat Pump: Thermal-Economic Modeling and Optimization**, *Energy Conversion and Management*, **51(12)**: 2600-2612 (2010).
- [27] Lemmon E., Huber M., Maclinden M., “**NIST Standard Reference Database 23: Reference Fluid Thermodynamic and Transport Properties-REFPROP**”, Version 10.0, National Institute of Standards and Technology. Standard Reference Data Program, Gaithersburg, (2018).
- [28] International du Froid., R600a, “**Isobutane: Thermophysical Properties**”, Institut International Du Froid = International Institute of Refrigeration., Paris, (2020).
- [29] Lemmon, E.W., “**Thermophysical Properties of Fluid Systems**”. NIST Chemistry WebBook, 1998.
- [30] Kakac S., Liu H., Pramuanjaroenkij A., “**Heat Exchangers: Selection, Rating, and Thermal Design**”, (2020): CRC Press.
- [31] Ontario Ministry of the Environment, March 2013, Published: February 26, 2017, Updated: August 16, (2021), <https://www.ontario.ca/page/earth-energy-systems-ontario> [32]
- [32] “**Iran Power Price**”. *Iran Minist. Energy, Inf. Cent.* (2021); Available from: https://www.globalpetrolprices.com/Iran/electricity_prices/.
- [33] Rohsenow W.M., Hartnett J.P., Cho Y.I., “**Handbook of Heat Transfer**”. Vol. 3., McGraw-Hill New York. (1998).
- [34] Eberhart R., Kennedy J.. “**A New Optimizer Using Particle Swarm Theory**”. in *MHS'95. Proceedings of the Sixth International Symposium on Micro Machine and Human Science*. Ieee (1995).
- [35] de Almeida B.S.G., Leite V.C., “**Particle Swarm Optimization: A Powerful Technique for Solving Engineering Problems**”, in *Swarm Intelligence-Recent Advances, New Perspectives and Applications*. (2019), IntechOpen.
- [36] Kheshti M., Ding L., **Particle Swarm Optimization Solution for Power System Operation Problems**, *Particle” Swarm Optimization with Applications*, p. 25-40 (2018).
- [37] **Iran Weather and Climate Data**. *Iran Meteorol. . Organ. Minist. Road Urban Dev.* (2020); Available from: <http://www.irimo.ir/far/>.
- [38] **Statistical Results of Energy Carriers’ Consumption in Residential areas in Iran**. (2020), Available from: <http://www.amar.org.ir/Default.aspx?tabid=73&Prodid=144>.
- [39] “**Iranian National Standards for Buildings, Topic.19: Building Envelop, Building Envelop**”, *Ministry of Road and Urban Development*, . Tehran., 2010.
- [40] **EnergyPlus**. (2020); Available from: <https://www.energy.gov/eere/buildings/downloads/energyplus-0>.
- [41] Heating A.S.O., **Thermal Environmental Conditions for Human Occupancy**, American Society of Heating, Refrigerating and Air-Conditioning Engineers, Vol. 55 (2004).
- [42] Varamarzyar M., Habibi M., Jafari J., Barati, A., **An Empirical Investigation of a Modified Gas Engine Heat Pump in Heating and Cooling Mode for the Residential Application**, *Iran. J. Chem. Chem. Eng. (IJCCE)*, **39(5)**: 321-332 (2020).
- [43] Ghasemi S.E., Ranjbar A.A., Hosseini S.M.J., **Cooling Performance Analysis of Water-Cooled Heat Sinks with Circular and Rectangular Minichannels Using Finite Volume Method**, *Iran. J. Chem. Chem. Eng. (IJCCE)*, **37(2)**: 231-239 (2018).
- [44] Norouzi N., Bashash Jafarabadi Z., Valizadeh Gh., Hemmati M.H., Khajepour H., **Energy, Exergy, and Exergoeconomic (3E)Analysis of Gas Liquefaction and Gas Associated Liquids Recovery co-process Based on The Mixed Fluid Cascade Refrigeration Systems**, *Iran. J. Chem. Chem. Eng. (IJCCE)*, **41(4)**:1391-1410 (2022).

- [45] Ahmadi, S., Nasr, R., [Comparative Study and Multi-Objective Optimization of Various Configurations in Natural Gas Liquefaction Process](#), *Iran. J. Chem. Chem. Eng. (IJCCE)*, **40(6)**: 1985-1995 (2021).